

FIRN EDGE AND EQUILIBRIUM LINE DETECTION USING SATELLITE SAR

R.V. Engeset

Norwegian Water Resources and Energy Directorate, Box 5091 Maj., N-0301 Oslo, Norway.

Tel: +47 22959595, fax: +47 22959590, email: rue@nve.no, Internet: www.nve.no

ABSTRACT

Glacier mass balance responds to changes in climate and may be used as a proxy indicator. However, several obstacles oppose mass balance change detection using field observations and optical remote sensing techniques at high latitudes. To overcome these problems we investigated the capability of satellite SAR to detect changes in mass balance and glacier facies. Eight years of winter ERS SAR data from Kongsvegen, Svalbard, were analysed. The results indicate that variations in mass balance cannot be retrieved from winter SAR backscatter imagery on an annual basis. The distinct zones observed in winter SAR imagery are firstly the firn accumulation zone, and secondly a low backscatter zone. The first zone is the part of the glacier where accumulation is in the form of firn metamorphism, while the second zone incorporates the superimposed ice accumulation area and ablation area. The firn edge altitude (FEA) was automatically retrieved for 31 of the 40 glaciers. The FEA did not change from year to year and gave a time-averaged value. The mapping method for firn edge detection was robust and can be used to produce a baseline data set with which to detect and measure future changes. The lower backscatter zone could be divided into two sub-zones. Separation was not equally easy from year to year, and no simple and robust retrieval method was found. The boundary between these two sub-zones did not migrate up and down the glacier from year to year, as would be expected if it corresponded to the lower limit of the late-autumn superimposed ice zone and the equilibrium line. This boundary could be detected on 20 of the 40 glaciers, and corresponded to the estimated mean equilibrium line altitude.

INTRODUCTION

Background

Global climate change is believed to have an early and large response at high latitudes (e.g. 1), and thus proxy observations on climate change in the Arctic region could serve as an early-warning system for global climate change (2). Climate change has a strong impact on the Arctic ice masses and mass balance. Recent studies show that the average glacier mass loss corresponds to the overall effects of human-induced greenhouse forcing and that the overall glacier decrease shows an accelerating trend (3). Furthermore, glacier dynamics and runoff respond to changes in mass balance (e.g. 4, 5). Also, increased melting of mountain glaciers and ice caps have caused a significant part of the observed global sea-level rise. It is believed that this effect will continue in the future (6, 7, 8). The mass balance of glaciers in the Arctic is difficult to observe due to the remote location, vast areas, harsh weather conditions and difficult logistics. Svalbard, with its geographical location and abundance of glaciers is an optimal place for this type of study, but direct mass balance observations from the Svalbard archipelago are few and no new traditional observation programmes are foreseen. The Arctic receives no sunlight during mid-winter and clouds frequently hinder data collection by optical sensors (9, 10), thus active microwave instruments represent promising tools for data collection. Synthetic aperture radar (SAR) images the Earth using a self-generated emitted electromagnetic pulse, which eliminates the problems of persistent cloud cover and dark winters. Furthermore SAR, with a wavelength of about 6 cm (such as on ERS-1/2, Radarsat and the upcoming Envisat) is sensitive to volume and surface scattering in the upper layer of the glacier and thus to surface and

near-surface structures related to the accumulation, ablation and metamorphism of snow and firn. Hence, SAR imaging of glaciers may be used for identifying properties related to mass balance and glacier facies. Promising results have been demonstrated by satellite remote sensing, with radar techniques (11, 12, 13, 14, 15, 16, 17) as well as optical techniques (e.g. 18, 19). However, in earlier studies using optical satellite data, localisation of the equilibrium line has been shown to be difficult on many of the smaller glaciers on Svalbard due to the widespread presence of superimposed ice (20).

Several authors point out that SAR appears to be a suitable tool for mapping the position of the equilibrium line (EL) using data from late in the ablation season (e.g. 21, 22, 16) or during dry-snow conditions during the winter (e.g. 13, 14). This would provide an important tool for monitoring the EL altitude (ELA), which is well correlated with annual net balance (e.g. 23, 24, 25, 26). The power of such a tool is shown by the impact of glacier mass balance on changes in sea level, water balance and climate. Although suggested from results on other glaciers, (14) show that detection of the EL using late autumn ERS SAR imagery is not possible over the glacier Kongsvegen, Svalbard. However, two distinct zones corresponding precisely to the accumulation and ablation areas, are identified in winter SAR imagery from the winter 1993/1994. The capacity of SAR to detect annual EL position and altitude is suggested in several studies (e.g., 27, 28, 13, 14, 15). However, most studies rely on one or two years of SAR data and a limited set of ground observations.

Research Objectives

The principal hypothesis to test in this work was if ERS SAR could be used to detect the equilibrium line. Furthermore, the mapping capacity of ERS SAR to detect glacier facies, in particular to map the extent of the firn accumulation area, the firn edge, the superimposed ice and glacier ice surface areas. Eight years of ERS SAR winter data were used to test the hypotheses.

The proposed methodology could be a positive contribution to the proposed Global Climate Observing System/Global Terrestrial Observing System (GCOS/GTOS, cf. 29) and the European Global Monitoring for the Environment and Security (GMES) programme, if the key glacier parameters are successfully retrieved.

METHODS

Svalbard and the Kongsvegen Glacier Study Areas

The Svalbard archipelago is situated between 76° – 81° North and 10° – 35° East. The non-glaciated areas have continuous permafrost. On the western coast of the largest island, Spitsbergen, the average annual temperature is about –6 °C and annual precipitation is about 400 mm (9, 30). The area receives continuous daylight for about four months during summer and is in continuous darkness for nearly four months during winter. Maximum cloudiness occurs in the summer, when more than one out of two days are overcast. Precipitation is mainly carried by the westerlies and is low due to the generally stratigraphically stable and low-moisture bearing air masses. About 60 percent of the land area is glacierised.

The glacier Kongsvegen at 78° 50' North and 13° East (see Figure 1) was selected for the detailed analysis in this work as this is the only large glacier on Svalbard with an annual mass balance observation series of some length (since 1986). The glacier is about 25 km long, has an area of 105 km², and an even surface of low slope (0.5° to 2.5°) going from sea level to 800 m above sea level (a.s.l.). The glacier is polythermal with a 50 to 200 m deep cold surface layer in the ablation area and temperate ice elsewhere (for a more detailed description of the glacier and previous work, see (31) and (32). Kongsvegen is one of several glaciers calving into Kongsfjorden, which is the fjord north of the peninsula Brøggerhalvøya.

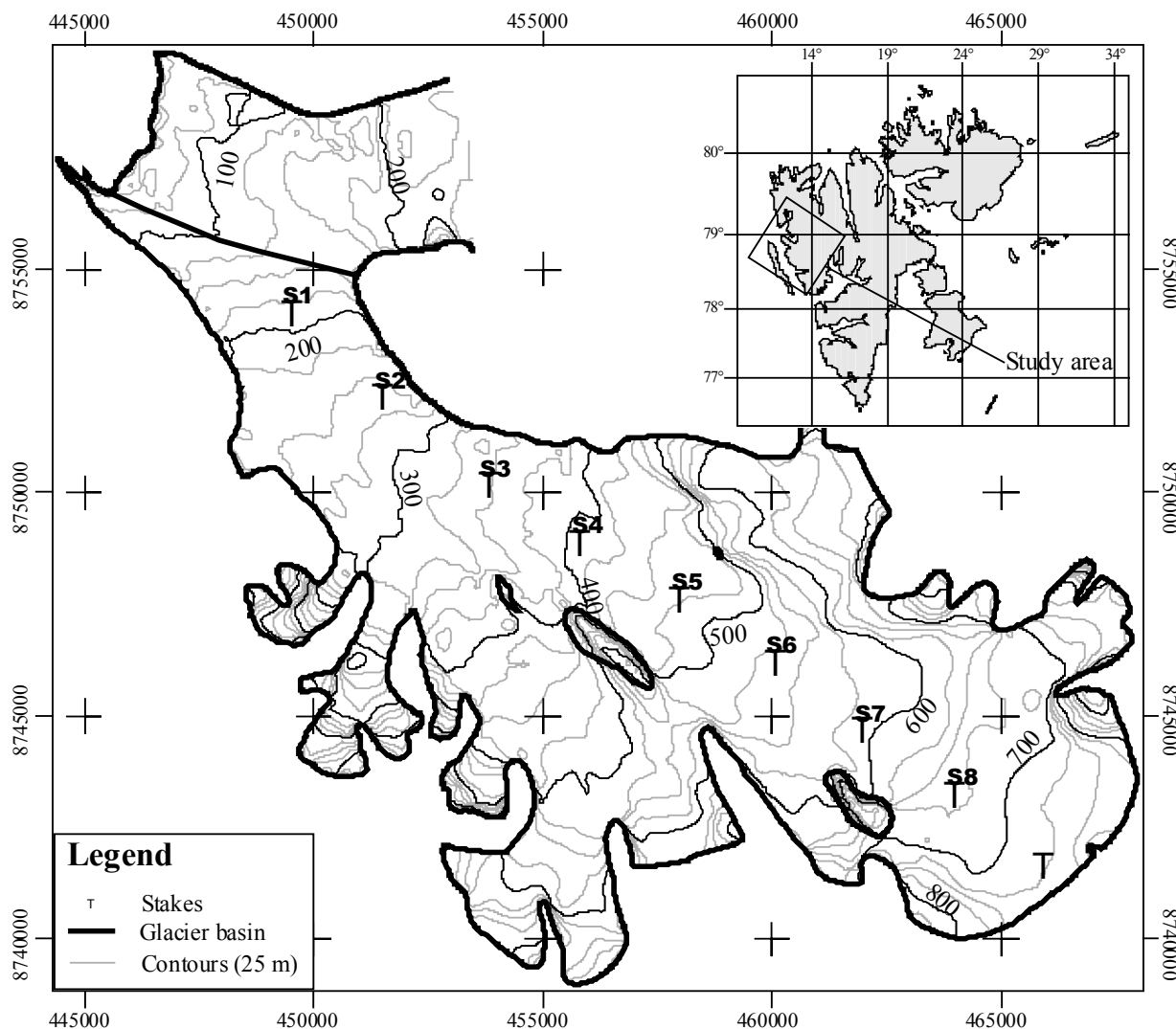


Figure 1: Maps of Svalbard (inset, full SAR-frame coverage is indicated as the study area) and Kongsvegen glacier. Kongsvegen flows westwards. Contours and location of stakes for mass balance observations are shown. The map of Kongsvegen is given in the UTM projection and co-ordinate system (figures in meters). Data are from the Norwegian Polar Institute.

ERS SAR Data

Data from the First and Second European Remote Sensing Satellites (ERS-1/2) are available since the winters of 1991/92 (which corresponds to the mass balance year 1991) and 1995/96 respectively. A set of SAR Precision Image (PRI) data from the ESA SAR Processing and Archiving Facilities in the UK (UK-PAF) were selected according to Table 1.

All images were repeat-pass (except the 1999 image from a nearby pass) acquisitions in a descending path. The PRI data were calibrated according to (33). The calibration procedure included corrections for antenna pattern, range-spread-loss and image geometry, all carried out by the UK-PAF. The SarToolBox software provided by ESA was applied to include reference replica power (ERS-1 data only), ADC saturation and PRI calibration constant corrections. (34) report very high analogue-to-digital conversion (ADC) power losses in the range from 2 (ERS-2) to 4 (ERS-1) dB over high backscatter ice regions such as glacier firn areas during winter. However, if correctly calibrated, Meadow et al. (1998) state that the results from ESA calibration and validation work show

that no degradation has occurred in the performance of the ERS-1 and 2 SARs with time. Thus time-series of correctly calibrated ERS SAR data are suitable for studying backscatter changes caused by changes in the land surface. Sub-scenes covering Kongsvegen were extracted and transformed into the UTM co-ordinate system and projection in which 20 m contours, stakes and glacier boundaries are available. Twelve ground-control points were used to tie the images to UTM coordinates. The images were projected into UTM using a second order transformation and nearest-neighbour resampling, after being first shifted to align. No digital terrain model was used for geocoding since a relatively small horizontal displacement error is expected from the glacier surface of Kongsvegen, which is flat with local slope between 2 and 3 degrees over most of the surface. Speckle was reduced by a 5 by 5 average moving-window filter.

The SARs on board the ERS satellites operate at a frequency of 5.3 GHz (equal to a wavelength of 5.66 cm in vacuum) and emit and receive with vertical polarisation. The incident angle on a horizontal surface at the centre of the swath is 23 degrees. The 3-look PRI data are in ground-range projection and have a pixel spacing of 12.5 m by 12.5 m. A full scene covers approximately 100 km by 100 km.

Table 1: ERS-1/2 SAR PRI data and calibration procedure. Antenna pattern, range-spread loss and image geometry corrections were carried out by the UK-PAF. STBX denotes further corrections carried out according to (33) using ESA SarToolBox software (URL http://earth1.esrin.esa.it/STBX/sartoolbox_home.html).

Date	Satellite	Orbit	Track	Calibration correction		
				PRI calibration const. K	Reference replica power	ADC saturation
1992 04 30	ERS-1	0413 3	481	STBX	STBX	STBX
1993 02 04	ERS-1	0814 1	481	STBX	STBX	STBX
1993 12 16	ERS-1	1265 0	481	STBX	STBX	STBX
1995 04 08	ERS-1	1950 7	481	STBX	STBX	STBX
1996 02 17	ERS-1	2401 6	481	STBX	STBX	STBX
1997 03 09	ERS-2	0985 4	481	STBX	No	STBX
1998 03 29	ERS-2	1536 5	481	STBX	No	STBX
1999 05 01	ERS-2	2106 2	166	STBX	No	STBX

Support Data

Mass balance has been measured at Kongsvegen since autumn 1986 using nine stakes along a 20 km long centre-profile on the glacier (e.g., 35). Accumulation is in the form of snow during the winter and the formation of superimposed ice. Ablation is in the form of melting of glacier ice, superimposed ice, snow and firn. Transformation of snow to glacier ice takes place through metamorphism, described by e.g. (36). Above the EL, accumulation dominates and contributions are given by both formation of superimposed ice and remaining winter snow at the end of the ablation season. For the observation period from 1987 to 1997, mean specific balances were 0.81 m water equivalent (w.e.) in the winter and -0.71 m w.e. in the summer, which gave a low but positive net balance of

0.10 m w.e. The equilibrium line altitude (ELA) ranges from 355 to 570 m a.s.l. during the observation period, which corresponds to fluctuation of the EL within a zone of nearly 9 km along the centre-profile. The average ELA was 505 m a.s.l., which was 1.5 km towards the glacier front from stake S6.

A meteorological station is operated at Ny-Ålesund, which is situated at sea level approximately 15 km west of the terminus of Kongsvegen. Observations of temperature and precipitation were used to select SAR acquisitions, which corresponded to periods when the upper layer of snow and firn was thought to contain no liquid water.

Vertical aerial photographs were acquired over Kongsvegen during August 1990 at 1:50,000-scale and during August 1995 at 1:30,000-scale. The photographs showed no fresh snow on the surface, except over high elevations. The distribution of exposed firn, superimposed ice and glacier ice was readily identified in the photographs.

The only map that covers the whole glacier is a Norwegian Polar Institute 1:100,000-scale map with 50 m contours and showing glacier boundaries. Also a digital elevation model (DEM) of 50 m grid-spacing was available. The DEM was constructed from different sources as described in (32). Stakes were positioned using high-precision static global positioning system (GPS) surveying methods (37). Repeated surface profiling with high-precision GPS receivers had been carried out during spring 1992 and 1996 (37).

Ground penetrating radar (GPR) data had been collected using a GSSI SIR-2 system with a 500 MHz frequency antenna. The observations were carried out in May 1996 and map near-surface structures, such as the interface between snow and glacier ice in the ablation area and annual firn layers in the accumulation zone.

Development of the Glacier Near-Surface Structures

Most Svalbard glaciers are polythermal with a cold surface layer of sub-zero temperatures in the ablation area, and temperatures at the pressure melting point in the accumulation zone. At the end of the winter, Kongsvegen is covered by a snow layer that normally varies in thickness from 0.7 m in the lower parts to 2.6 m in the upper parts. The specific winter balance ranges from 0.5 to 1.2 m water equivalents (w.e.) in the observation period. Up to 400-600 m a.s.l., all the winter snow is lost by ablation exposing a surface of glacier ice. As the glacier ice is composed of large grains, which are covered by dirt and subject to erosion by melt water on the surface, an uneven surface develops during the ablation season. In this text, glacier ice denotes ice that is transported deep into the glacier, in order to separate such ice from superimposed ice, which has different characteristics. Meteorological processes such as irradiation, wind and precipitation govern the structure of the ice surface as frozen in the early winter. The local climatic conditions at the very end of the ablation season may alter the surface roughness considerably. For instance, clear skies and high irradiation could produce a rough and crisp surface with much air between the ice grains. Rain, on the other hand, is thought to reduce the microscale roughness.

Accumulation, ablation and metamorphism of snow to firn and ice control the near-surface structure of glaciers. The metamorphism is strongly influenced by the temperature regime of the glacier. With regards to SAR observations of Svalbard glaciers it is worth pointing out the following two modes of metamorphism; that of firnification and that of superimposed ice formation. Snow turns into firn after one summer. Transformation of snow to firn and ice normally implies growth of snow grains into larger grains through processes such as packing, clustering and displacement of grains, refreezing and internal deformation. Liquid water is normally an effective agent in this process at some stage. The intermediate result of such a transformation is a volume of coarse grains, ice layers and lenses. On the other hand, superimposed ice forms rapidly when melt water accumulates on a non-permeable surface of sufficiently low temperature to freeze the melt water. These conditions develop at the glacier ice surface in the ablation area during the autumn and winter. The snow and

firm cover is normally thin and does not provide enough isolation to prevent heat loss and cooling of the glacier ice caused by the temperature gradient between the ice and the cold winter air.

Under cold ice conditions as discussed above, superimposed ice normally forms when air temperatures are above 0 °C and liquid water is provided by snowmelt or rain. The result of superimposed ice formation is a layer of ice on top of the glacier ice, normally formed during early summer but occasionally also during the rest of the year (J. O. Hagen, personal communication). Formation of superimposed ice is to a certain degree influenced by surface topography. Even on a relatively flat glacier surface such as that of Kongsvegen, superimposed ice formation is enhanced on relatively horizontal parts where lateral movement of melt water is limited.

Examples of the annual shifting of the ablation area, superimposed ice accumulation area and firn accumulation as a result of changing mass balance are shown in Figure 2.

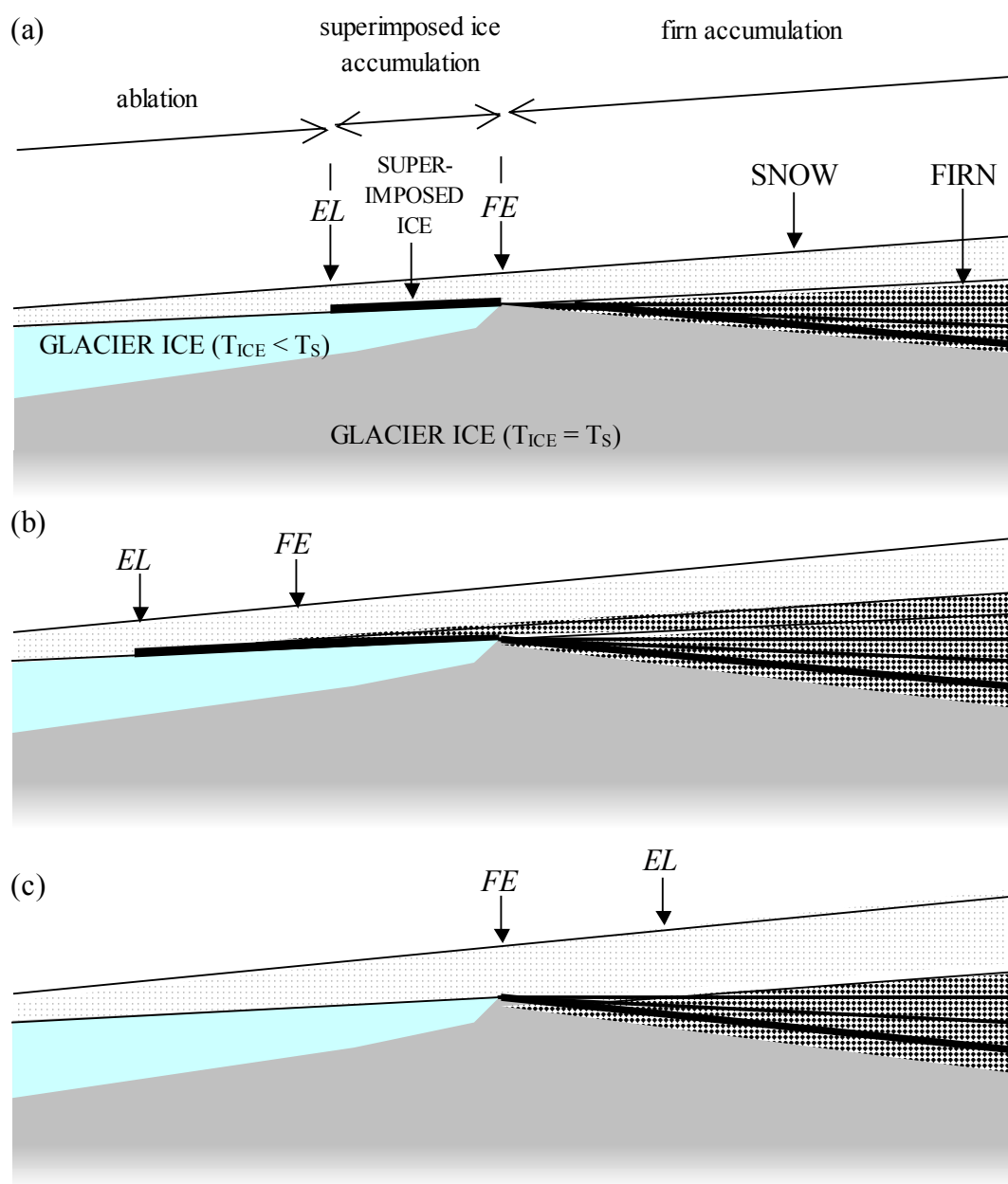


Figure 2: Schematic description of the near-surface stratigraphy during (a) normal, (b) positive, and (c) negative mass balance years. EL denotes the equilibrium line, FE the firn edge, T_S temperature at the pressure melting point and T_{ICE} the glacier ice temperature. The figures show the situation at the end of the winter with a snow cover on top.

Figure 2a shows the stratigraphy (facies) developed in a normal balance year. Under the winter snow layer three zones are identified, corresponding to glacier ice, superimposed ice and firn in this sequence going from low to high elevation. Superimposed ice forms where melt water encounters below-freezing temperatures in the sub-snow/firn ice.

To illustrate the effect of mass balance change from year to year on stratigraphy, Figure 2b and Figure 2c show the stratigraphic changes caused by a succeeding positive and negative year respectively. If followed by a positive mass balance year (as in Figure 2b), an extended superimposed ice area forms, and both the EL and the annual firn edge (FE) are located closer to the glacier front than in the previous year. If not only superimposed ice, a firn layer may form below the previous year's FE or even EL. If succeeded by a negative mass balance year (as in Figure 2c), the superimposed ice zone may disappear completely and the FE is closer to the glacier head than in the previous year. In any particular year, the near-surface stratigraphy will be the result of changes taking place over a number of years.

Radar Backscatter From Snow, Superimposed Ice and Glacier Ice During Winter

Dry winter snow absorbs very little energy in the absence of liquid water and is considered nearly loss-free at microwave frequencies. Thus, scattering at the air-snow interface can be neglected (38) and due to the large penetration depth, volume scattering by grains and inhomogeneities is the dominant backscatter mechanism (39) over the studied glacier areas. The winter snow cover normally developed at Kongsvegen is relatively thin and composed of fine grains due to the cold temperatures during the winter. Therefore it does not significantly modify the SAR power, which as a consequence is controlled by the sub-snow features (40).

Radar Backscatter from Superimposed Ice and Glacier Ice During Winter

In the parts of the glacier where the ice is exposed at the end of the preceding ablation season, backscatter at the snow-ice interface dominates. The backscatter strength for such surfaces largely depends on surface roughness. A surface is considered rough at C-band at surface height standard deviation greater than about one centimetre (41, 42), which is generally true for ablation ice surfaces (43).

Glacier ice is formed by the transformation from snow to ice by processes such as freeze-melt cycles, compaction and clustering under large pressure yielding large grains of ice with an ordered crystal orientation and sealed air inclusions between the grains. Exposed to melt water and ablation processes on the surface, glacier ice develops a rough surface on the centimetre scale. On the other hand, freezing of liquid water on a cold surface forms superimposed ice, which is more a homogeneous medium with random crystal orientation. Therefore, superimposed ice generally develops a smoother surface when exposed to surface ablation. Although these two types of ice may appear alike in the field, the smoother surface normally developed on superimposed ice could be used to separate these zones using SAR. Divergent findings are reported on the issue of SAR separability between superimposed ice and glacier ice surfaces. (44) oppose the possibility of separating these zones, while (45) report on observed differences due to surface roughness over a glacier on Svalbard. The different conclusions are possibly due to roughness differences as a consequence of different climatic conditions at the end of the ablation season.

Radar Backscatter from Firn During Winter

In the upper parts of the glacier where firn accumulation occurs, layers dominated by large firn grains and ice layers and lenses develop. In these areas, well-developed grains and ice structures are effective scattering elements on the ERS SAR wavelength and cause considerable volume scattering. Density changes associated with thin ice layers and lenses also cause reflections and scattering in this part. On Svalbard, no reports are available on the occurrence of a dry snow facies, as identified on Greenland ice sheet by (46). On the contrary, Svalbard glaciers are subject to melt also in

the upper parts of the accumulation area during the summer. The melt water percolates and provides a mechanism for rapid snow grain growth and thus reassembles the wetted snow and percolation facies, again using the terminology established by (46). Very high radar backscatter values over these facies have been reported from several studies (e.g. 12, 47, 13, 17), in the range from -4 to 0 dB. Return caused by volume scattering is largely independent of angle and uniform high backscatter from parts of glaciers is diagnostic for deep firn areas with no liquid water inclusions. (48) and (17) observed the top ten to thirty metres of several Svalbard glaciers using high-frequency GPR simultaneously with ERS SAR acquisitions during the spring. These studies show that the glacier signal in the SAR images is from the ice and firn structures below the winter snow layer.

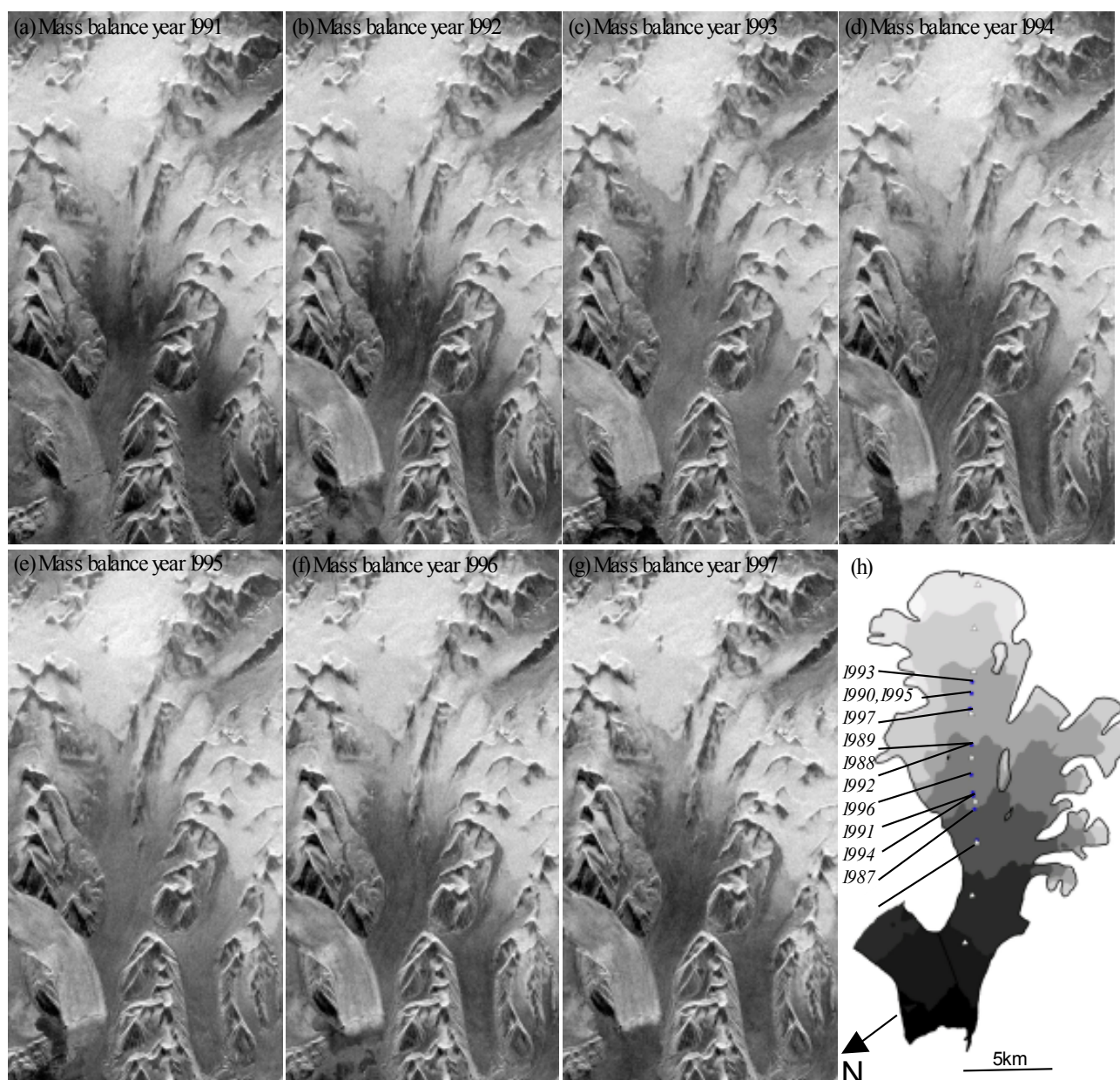


Figure 3: Calibrated ERS SAR PRI winter images over Kongsvegen from seven years (a-g). The annual position of the EL for the corresponding mass balance years is shown in h). The grey tones in h) show elevation intervals of 100 m. ERS SAR data are copyright European Space Agency.

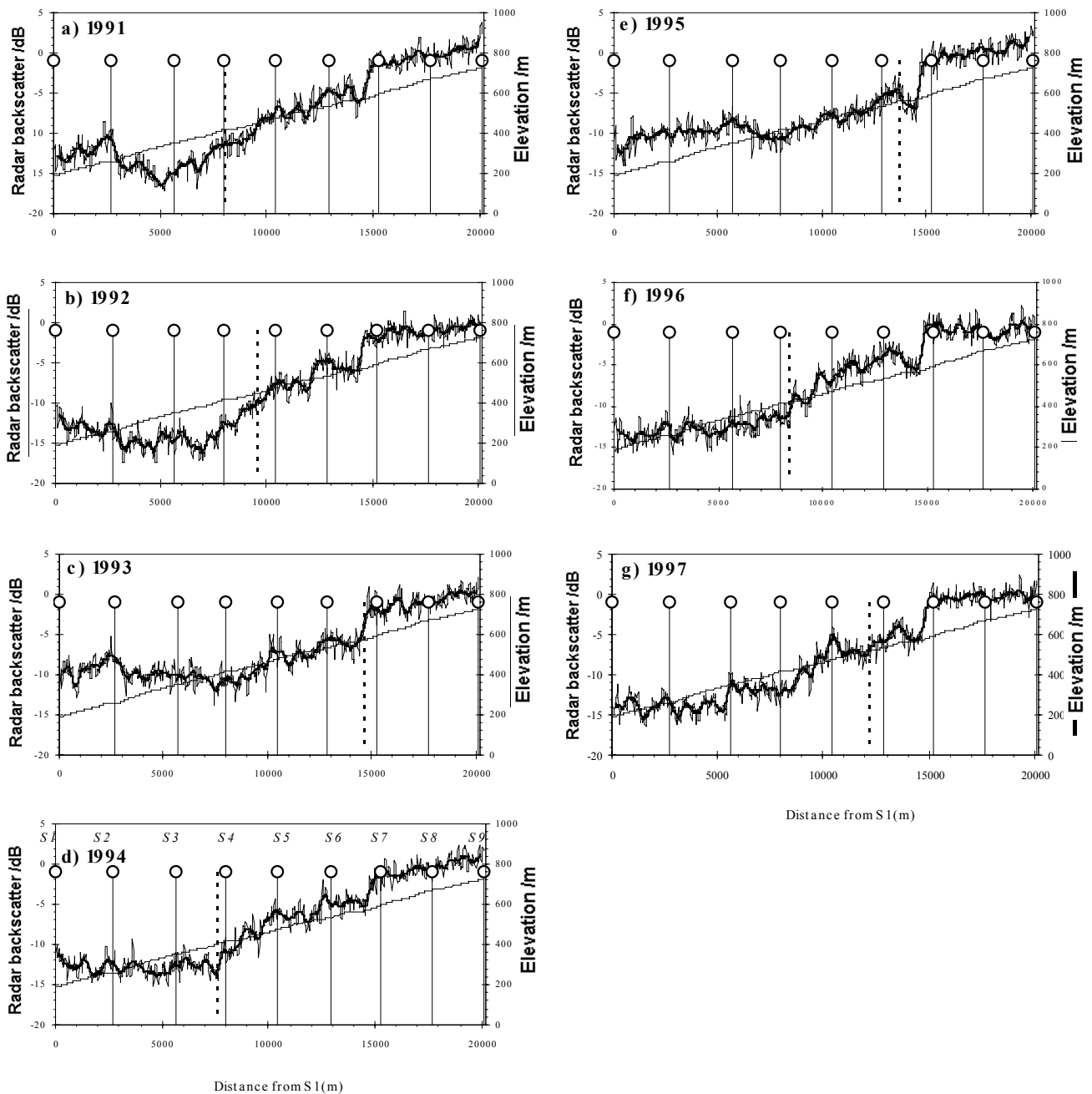


Figure 4: ERS SAR backscatter along the mass balance observation profile on Kongsvegen from seven years (a-g). The years refer to mass balance years, not SAR acquisition years. Two graphs show radar backscatter, the thin graph is from the SAR image convolved by a 5 x 5 average filter, and a 15-pixels running mean was applied to produce the thick graph. The stake positions are indicated with vertical lines with a superimposed circle, and the ELs with thick dashed lines.

3. RESULTS

Monitoring the Annual Equilibrium Line

Figure 3 shows the ERS SAR winter imagery over Kongsvegen for the mass balance years 1991 to 1997. Although inter-annual changes in backscatter were observed over the glacier area, the dislocation of the EL from one year to another, as suggested by the mass balance data, was not apparent in the SAR data. Calibrated SAR backscatter values extracted along the mass balance observation profile from stake S1 to stake S9 (see Figure 4) confirms this. Thus the hypothesis of EARSeL eProceedings No. 2

profile from stake S1 to stake S9 (see Figure 4) confirms this. Thus the hypothesis of the EL detection capability of ERS SAR was rejected as far as Kongsvegen is concerned.

One distinct and two less distinct zones are observed in the image series. The former corresponded to the typical firn accumulation area and this is further discussed below. The two zones further down the glacier were less separable and no typical threshold backscatter value emerged for identification of their boundaries. Differences in surface scattering at the (winter snow covered) glacier ice and superimposed ice surfaces are responsible for the changes in the low backscatter zones.

Monitoring the Firn Accumulation Area and Firn Edge

The upper zone (see Figure 3 and Figure 4) corresponds to the firn accumulation area and exhibits a time-invariant and very high backscatter values in the range -2 to 1 dB. Reconstruction of near-surface stratigraphy from stake, GPR and GPS observations showed that the very clear ERS SAR signal observed over Kongsvegen during winter conditions was associated with the formation of a multi-year firn volume whose depth increased to several metres within a horizontal distance of a few hundred metres. The firn volume is of considerable thickness over most of the glacier above stake S7 and thus the entire firn-accumulation area of the glacier provides a stable high-backscatter target year after year.

The perennial firn accumulation area could be automatically identified from the SAR imagery using a four-step algorithm; i) thresholding the backscatter image at -2.5 dB, ii) iterative speckle reduction until convergence, iii) edge detection, and iv) dilation. In step i), the backscatter threshold value was kept constant for all years and clearly separated firn accumulation areas from other parts of the glacier in a robust manner. No local incident angle correction was applied. Ascending and descending path acquisitions with a different incident angle were investigated over Kongsvegen, and incident angle effects were found to be small (14). Speckle reduction was carried out in step ii) in order to eliminate isolated pixels erroneously detected due to SAR image speckle (also correctly detected pixels may be discarded in this process). Steps iii) and iv) were carried out to produce a clear demarcation of the firn accumulation area.

Monitoring the Zone where the Equilibrium Line Fluctuates

A shift of about 4 to 5 dB in backscatter was observed near stake S7 between 14.2 and 14.7 km (i.e. near 570 m a.s.l.) from stake S1 and appeared to be a prominent feature of all years. The shift corresponded to an increase in backscatter from between -6 and -5 dB to a level between -1 and 0 dB. The shift was exceptional in that it was large and occurred in the same place each year. Effective volume scattering from firn grains was identified as the principal agent for the backscatter variation from year to year in the EL fluctuation zone and, in particular, the very high and rather constant backscatter observed over the upper areas of the glacier. Backscatter values as high as 0 dB were most likely caused by a high number of efficient scattering elements in a deep volume of firn. The backscatter strength is generally very high and rather constant over these parts of the glacier, although some spatial variation is observed.

To investigate the stability of SAR backscatter over different parts of the glacier from year to year, the temporal standard deviation of backscatter for the mass balance years from 1991 to 1997 was calculated along the profile from stake S1 to S9 (Figure 5). High temporal variability in backscatter (standard deviation of 2 dB) was apparent in the lower zone for all years in which the net balance was negative, below the minimum ELA over the SAR observation period. Above this point located 0.5 km below stake S4, SAR backscatter was relatively stable with a standard deviation of 1 dB. In summary, while the ELA maximum corresponded to a distinct up-glacier increase in SAR backscatter identified in all images, the ELA minimum corresponded to a distinct up-glacier decrease in temporal (perennial) stability in SAR backscatter.

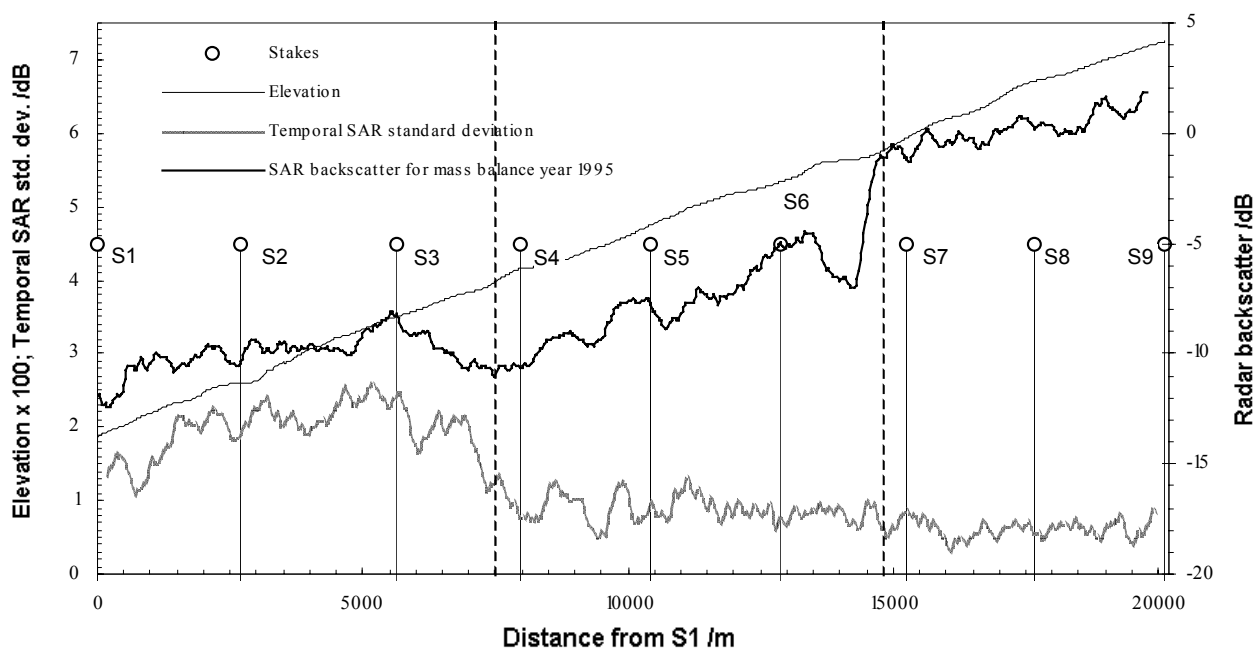


Figure 5: The top panel shows the temporal standard deviation of annual SAR backscatter, typical annual SAR backscatter (the example is from mass balance year 1995) and surface elevation along the stake centre-line. Minimum and maximum ELA is shown by vertical dashed lines.

Automatic Detection of the Firn Accumulation Area and Time-Averaged ELA Over a Full ERS SAR Frame

The firn accumulation area detection algorithm was applied to all images and successfully mapped the perennial (or rather average) firn accumulation area every year. Exactly the same parameter set was applied for each year. The technique was designed to be fairly simple in order to be easily transferable to an operational glacier monitoring system. The ERS SAR full-coverage scenes (Figure 6 shows the year 1995) were analysed to see if the findings from Kongsvegen were observable for other glaciers in the area. Only limited field data were available other than from the small glaciers Austre Brøggerbreen and Midre Lovénbreen – none of which have a well-developed firn accumulation area. The firn accumulation areas were mapped by applying the previously discussed firn edge detection algorithm on the winter images. The mean elevation of the firn edge was estimated for all glaciers larger than 15 km² within the SAR scene.

Although the annual EL position could not be mapped, the time-averaged position was estimated when a distinct zone of intermediate backscatter values could be identified. The mean lower elevation of this zone was taken to be the ELA based on the assumption that the intermediate backscatter level observed for this zone was attributable to superimposed ice and hence this zone is the lower part of the accumulation area. The determination of elevation was done by visual interpretation of the average position using the map series Svalbard 1:100,000 from the Norwegian Polar Institute. As no direct glaciological mass balance observations were available from the glaciers, the SAR-derived data were assessed based on the estimates by (30).

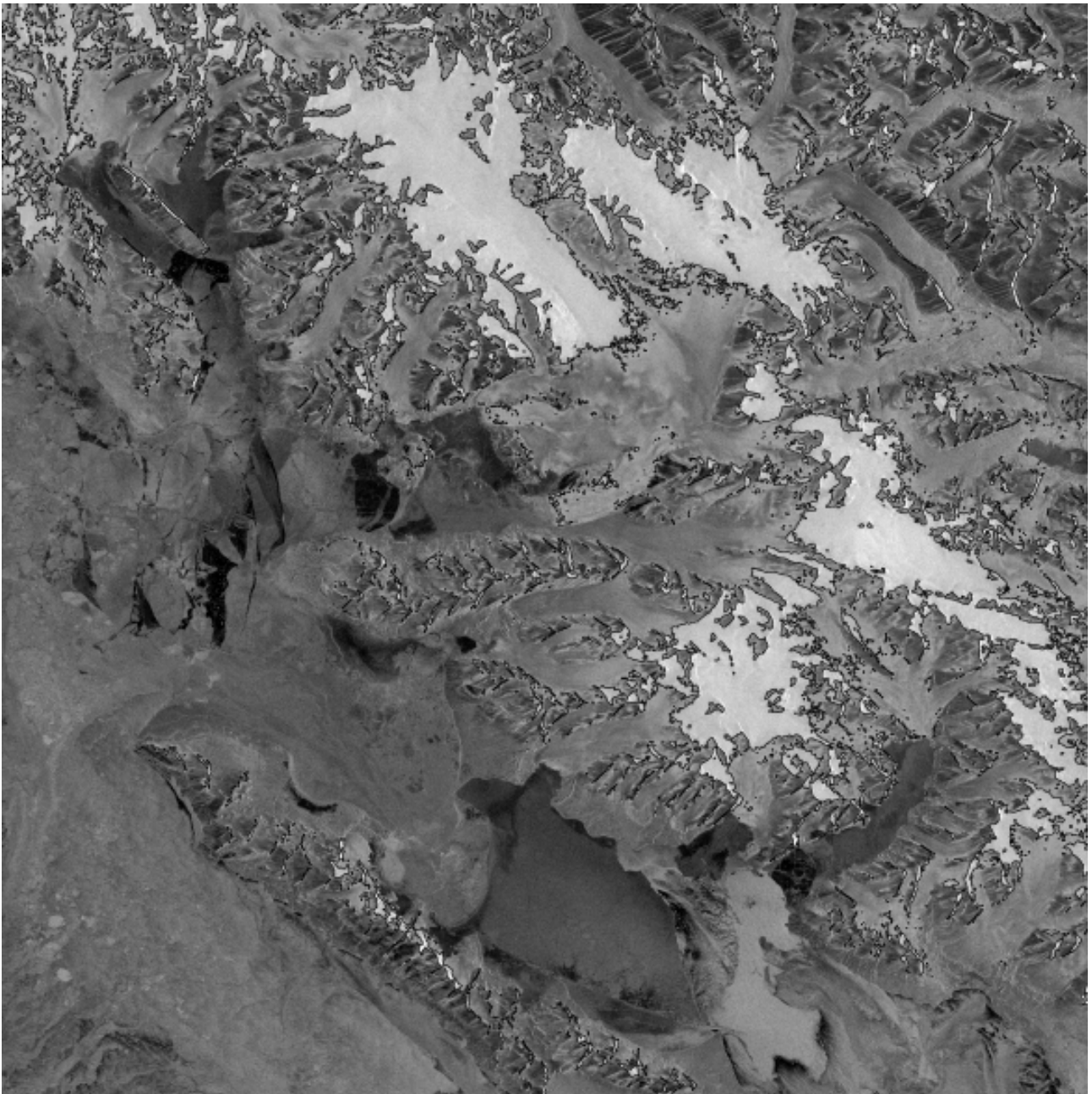


Figure 6: ERS SAR full-scene (100 x 100 km²) image over the Kongsfjorden area from mass balance year 1995. The black line delineates the firm accumulation boundary as retrieved using the automatic four-step detection algorithm (the technique is described in the text). ERS SAR data are copyright European Space Agency.

The results from the 31 glaciers where the firm edge altitude (FEA) could be retrieved are shown in Figure 7. The FEA was on average located some 170 m above the estimated ELA. Regression between SAR-derived and estimated ELA gave $r^2=0.80$. Although this correspondence was encouragingly high, unambiguous detection of the ELA using SAR may be difficult to automate and the procedure involved subjective interaction. These applications of SAR should be further investigated using geocorrected SAR images (e.g., 49), which also cover other parts of Svalbard.

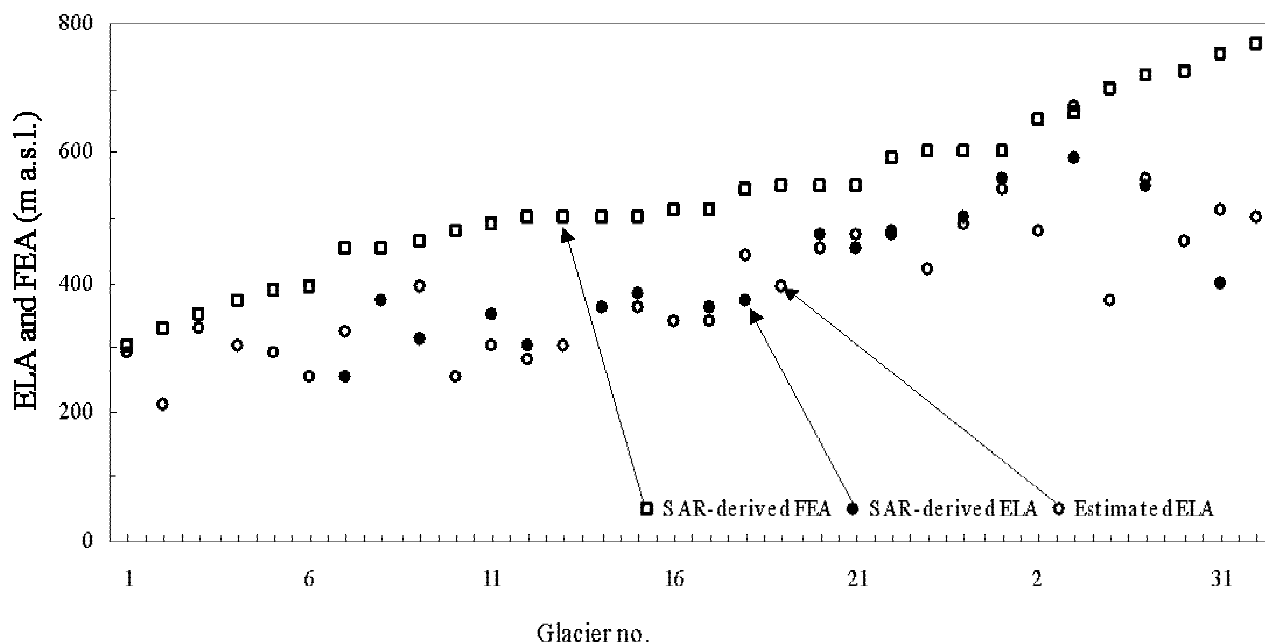


Figure 7: Relationship between equilibrium line altitude (ELA) and firn edge altitude (FEA). Estimated ELA was taken from (30). SAR-derived ELA and FEA were retrieved from ERS SAR image using the algorithm described in this paper.

CONCLUSIONS

This work on ERS SAR glaciers change detection and monitoring over Svalbard during wintertime shows that the annual position of the equilibrium line could not easily be retrieved from backscatter observations during winter. Secondly, the perennial firn accumulation area could be detected and mapped due to the extraordinary high backscatter over these parts of the glaciers as opposed to the superimposed ice and ablation areas, and the lower elevations of the accumulation area approximated the maximum elevation of the equilibrium line during the observation period. The inter-annual variation in backscatter below the minimum elevation of the equilibrium line during the observation period was double that over higher elevations.

The results from Kongsvegen suggested that the perennial interval (minimum and maximum) of equilibrium line altitudes could be mapped using ERS SAR during winter, but that the altitude of the annual equilibrium line could not be resolved. This suggests that we have a tool for glacier change detection and monitoring that is applicable over the Arctic region on a time-scale of some years.

ACKNOWLEDGEMENTS

The European Commission, Framework Programme IV, Environment and Climate Research Programme (DG XII), contract ENV4-CT97-0490 (additional support provided by relevant national councils, universities and related institutions) and the Norwegian Polar Institute covered the costs of the ERS SAR data, which were provided by ESA on a research and demonstration grant. Dr. Jack Kohler, Dr. Kjetil Melvold., Prof. Bengt Lundén, Prof. Jon Ove Hagen, Dr. Dan Johan Weydahl, Mr. Max König, Dr. Jan-Gunnar Winther and Dr. Miriam Jackson made valuable contributions. Prof. Helgi Björnsson and Prof. em. Olav Liestøl stimulated discussions during the initial phases of this work. An anonymous referee is acknowledged for a constructive review.

REFERENCES

1. Hartmann, D.L., 1994, Global physical climatology. Academic Press. San Diego, California, U.S.A.
2. Houghton, J.T., Meira Filho, L.G., Callander, B.A., Harris, N., Kattenberg, A., and Maskell, K. 1995, Climate change 1995 – The Science of Climate Change. Cambridge University Press, Cambridge, U.K.
3. Haeberli, W., Frauenfelder, R., Hoelzle, M., and Maisch, M., 1999, On rates and acceleration trends of global glacier mass changes. *Geografiska Annaler*, 81A(4), 585-591.
4. Laumann, T., and Reeh, N., 1993, Sensitivity to climate change of the mass balance of glaciers in southern Norway. *Journal of Glaciology*, 39(133), 656-665.
5. Jóhannesson, T., 1997, The response of two Icelandic glaciers to climatic warming computed with a degree-day glacier mass balance model coupled to a dynamic glacier model. *Journal of Glaciology*, 43(144), 321-327.
6. Meier, M.F., 1984, Contributions of small glaciers to global sea level. *Science*, 226(4681), 1419-1421.
7. Warrick, R.A., Le Provost, C., Meier, M.F., Oerlemans, J., and Woodworth, P.L., 1996, Changes in sea level. In Houghton, J.T., Meira Filho, L.G., Callander, B.A., Harris, N., Kattenberg, A., and Maskell, K., (eds.), *Climate Change 1995 – The Science of Climate Change*. Cambridge University Press, Cambridge, 358-405.
8. Zuo, Z., and Oerlemans, J., 1997, Contribution of glacier melt to sea-level rise since AD 1865: a regionally differentiated calculation. *Climate Dynamics*, 13, 835-845.
9. Hanssen-Bauer, I., Kristensen Solås, M., and Steffensen, E.L., 1990, The climate of Spitsbergen. The Norwegian Meteorological Institute Report, 39/90.
10. Marshall, G.J., Rees, W.G., and Dowdeswell, J.A., 1993, Limitations to multitemporal visible band satellite data from polar regions imposed by cloud cover. *Annals of Glaciology*, 17, 113-120.
11. Fahnestock, M.A., Bindschadler, R., Kwok, R., and Jezek, K., 1993, Greenland ice sheet surface properties and ice dynamics from ERS-1 SAR imagery. *Science*, 262, 1530-1534.
12. Jezek, K.C., Drinkwater, M.R., Crawford, J.P., Bindschadler, R., and Kwok, R., 1993, Analysis of synthetic aperture radar data collected over the southwestern Greenland ice sheet. *Journal of Glaciology*, 39(131), 119-132.
13. Rees, W.G., Dowdeswell, J.A., and Diament, A.D., 1995, Analysis of ERS-1 synthetic aperture radar data from Nordaustlandet, Svalbard. *International Journal of Remote Sensing*, 16(5), 905-924.
14. Engeset, R.V., and Weydahl, D.J., 1998, Analysis of glaciers and geomorphology on Svalbard using multitemporal ERS-1 SAR images. *IEEE Transactions on Geoscience and Remote Sensing*, 36(6), 1879-1887.
15. Partington, K.C., 1998, Discrimination of glacier facies using multi-temporal SAR data. *Journal of Glaciology*, 44(146), 42-53.
16. Brown, I.A., Kirkbride, M.P., and Vaughan, R.A., 1999, Find the firn line! The suitability of ERS-1 and ERS-2 SAR data for the analysis of glacier facies on Icelandic icecaps. *International Journal of Remote Sensing*, 20(15/16), 3217-3230.
17. Engeset, R.V., and Ødegård, R.S., 1999, Comparison of annual changes in winter ERS-1 SAR images and glacier mass balance of Slakbreen, Svalbard. *International Journal of Remote Sensing*, 20(2), 259-271.
18. Østrem, G., 1975, ERTS data in glaciology – an effort to monitor glacier mass balance from satellite imagery. *Journal of Glaciology*, 15(73), 403-415.

19. Williams, R.S., Hall, D.K., and Benson, C.S., 1991, Analysis of glacier facies using satellite techniques. *Journal of Glaciology*, 37(125), 120-128.
20. Winther, J-G., 1993, Landsat TM derived and in situ summer reflectance of glaciers in Svalbard. *Polar Research*, 12, 37-55.
21. Smith, L.C., Forster, R.R., Isacks, B.L., and Hall, D.K., 1997, Seasonal climatic forcing of alpine glaciers revealed with orbital synthetic aperture radar, *Journal of Glaciology*, 43(145), 480-488.
22. Kelly, R.E.J., Engeset, R., Kennett, M., Barrett, E. C., and Theakstone, W., 1997, Characteristic snow and ice properties of a Norwegian ice cap determined from complex ERS SAR. *Proceeding of 3rd ERS Symposium (ESA)*, 18-21 March 1997, Florence, Italy.
23. Liestøl, O., 1967, Storbreen glacier in Jotunheimen. *Norsk Polarinstitutt Skrifter*, 141.
24. Schytt, V., 1981, The net mass balance of Storglaciären, Kebnekaise, Sweden, related to the height of the equilibrium line and to the height of the 500 mb surface. *Geografiska Annaler*, 63A(3-4), 219-223.
25. Hagen, J.O., and Liestøl, O., 1990, Long-term glacier mass-balance investigations in Svalbard 1950-88. *Annals of Glaciology*, 14, 102-106.
26. Østrem, G., and Brugman, M., 1991, Glacier mass balance measurements. A manual for field and office work. Environment Canada, Saskatoon, Canada, National Hydrology Research Institute. (NHRI Science Report 4.)
27. Lingle, C.S., Harrison, W.D., Ahlnäs, T.K., Heinrichs, T.A., and Roush, J.J., 1992, Observation of Alaskan glaciers with ERS-1 synthetic aperture radar. In paper presented at the Alaskan SAR Facility (ASF) Users Meeting, 29-29 July 1993, Seattle, Washington, U.S.A.
28. Hall, D.K., Williams, R.S., Jr., and Sigurdsson, O., 1995, Glaciological observations of Brúarjökull, Iceland, using synthetic aperture radar and thematic mapper satellite data. *Annals of Glaciology*, 21, 271-276.
29. WMO, 1997, CGOS/GTOS plan for terrestrial climate-related observation. GCOS 32, Version 2.0, WMO/TD, 796, UNEP/DEIA/TR, 97-7.
30. Hagen, J.O., Liestøl, O., Roland, E., and Jørgensen, T., 1993, Glacier atlas of Svalbard and Jan Mayen. *Norsk Polarinstitutt Meddelser*, 129.
31. Björnsson, H., Gjessing, Y., Hamran, S.-E., Hagen, J.O., Liestøl, O., Pálsson, F., and Erlingson, B., The thermal regime of sub-polar glaciers mapped by multi-frequency radio echosounding. *Journal of Glaciology*, 42(140), 23-32.
32. Melvold, K., and Hagen, J.O., 1998, Evolution of a surge-type glacier in its quiescent phase: Kongsvegen, Spitsbergen, 1964-95. *Journal of Glaciology*, 44(147), 394-404.
33. Laur, H., Bally, P., Meadows, P., Sanchez, J., Schaettler, B., Lopinto, E., and Esteban, D., 1998, ERS SAR calibration. Derivation of the backscatter coefficient s^0 in ESA ERS PRI products. ESA document no. ES-TN-RS-PM-HL09, Issue 2, Rev. 5b, September 1998, ESA/ESRIN.
34. Meadows, P.J., Laur, H., and Schättler, B., 1998, The calibration of ERS SAR imagery for land applications. *Proceeding of 2nd International Workshop on Retrieval of Bio- and Geophysical Parameters from SAR Data for Land Applications*, Noordwijk, The Netherlands, 21-23 October 1998, ESA Publication SP-441.
35. Hagen, J.O., Melvold, K., Eiken, T., Isaksson, E., and Lefauconnier, B., 1999, Mass balance methods on Kongsvegen, Svalbard. *Geografiska Annaler*, 81A(4), 593-601.
36. Paterson, W.S.B., 1994, *The physics of glaciers*. 3rd ed., Pergamon Press, Oxford.
37. Eiken, T., Hagen, J.O., and Melvold, K., 1997, Kinematic GPS survey of geometry changes on Svalbard glaciers. *Annals of Glaciology*, 24, 157-163.

38. Ulaby, F.T., Moore, R.K., and Fung, A.K., 1983, Microwave remote sensing: active and passive. Volume III. Addison-Wesley, Reading, Massachusetts.
39. Mätzler, C., Aebischer, H., and Schanda, E., 1984, Microwave dielectric properties of snow. IEEE Journal of Oceanic Engineering, OE9(5), 366-371.
40. Rott, H., and Mätzler, C., 1987, Possibilities and limits of synthetic aperture radar for snow and glacier surveying. Annals of Glaciology, 9, 195-199.
41. Guneriusson, T., Johnsen, H., and Sand, K., 1996, DEM corrected ERS-1 SAR data for snow monitoring. International Journal of Remote Sensing, 17(1), 181-195.
42. Sabins, F.F., Jr., 1997, Remote sensing: principles and interpretation, 3rd ed., Freeman, New York.
43. Rott, H., 1984, The analysis of backscattering properties from SAR data of mountain regions. IEEE Journal of Ocean Engineering, OE9(5), 347-355.
44. Bindschadler, R., and Vornberger, P., 1992, Interpretation of SAR imagery of the Greenland ice-sheet using coregistered TM imagery. Remote Sensing of Environment, 42(3), 162-175.
45. Marshall, G.J., Rees, W.G., and Dowdswell, J.A., 1995, The discrimination of glacier facies using multi-temporal ERS-1 SAR data. In ASKNE, J., (ed.), Sensors and Environmental Applications of Remote Sensing, Balkema, Rotterdam, The Netherlands, 263-269.
46. Benson, C.S., 1961, Stratigraphic studies in the snow and firn of the Greenland Ice Sheet. Folia Geographica Danica, 9, 13-37.
47. Rott, H., Sturm, K., and Miller, H., 1993, Active and passive microwave signatures of Antarctic firn by mean of field measurements and satellite data. Annals of Glaciology, 17, 337-343.
48. Hamran S-E., Guneriusson, T., Hagen, J.O., and Ødegård, R., 1997, Ground penetration radar and ERS SAR data for glacier monitoring. Proceeding of IGARSS'97, Singapore, ISBN 0-7803-3836-7, 634-636.
49. Johnsen, H., Lauknes, I., and Guneriusson, T., 1995, Geocoding of fast-delivery ERS-1 SAR image mode product using DEM data, International Journal of Remote Sensing, 16(11), 1957-1968.